High resolution mapping of the recombination landscape of the phytopathogen Fusarium graminearum suggests two-speed genome evolution

High resolution mapping of the recombination landscape of the phytopathogen *Fusarium graminearum* suggests two-speed genome evolution

Benoit Laurent[1], Christos Palaiokostas[2], Cathy Spataro[1], Magalie Moinard[1], Enric Zehraoui[1], Ross D. Houston[2] and Marie Foulongne-Oriol[1]*

[1] MycSA, INRA, Université de Bordeaux, 33882 Villenave d'Ornon, France

[2] The Roslin Institute, University of Edinburgh, Midlothian EH25 9RG, Scotland, UK

*Corresponding author

Mailing address: INRA, UR1264 Mycologie et Sécurité des Aliments, bâtiment Qualis, 71 avenue Edouard Bourlaux, CS 20032 F-33882 Villenave d'Ornon cedex, France

Phone: +33 (0)5 57 12 26 35

Fax: +33 (0)5 57 12 25 00

Email : marie.foulongne-oriol@inra.fr

Keywords: *Gibberella zeae*, dense genetic linkage map, Genotyping-by-Sequencing, RAD-seq, meiosis, crossover rate

Running title: Recombination landscape of *Fusarium graminearum*.

Total word count: 6,992
Summary: 241
Introduction: 745
Results: 1,990
Discussion: 2,003
Experimental Procedures: 1,487
Acknowledgement: 82
Table & Figures legends: 444

This article has been accepted for publication and undergone full peer review but has not been through the copyediting, typesetting, pagination and proofreading process which may lead to differences between this version and the Version of Record. Please cite this article as an 'Accepted Article', doi: 10.1111/mpp.12524

Summary

Recombination is a major evolutionary force, increasing genetic diversity and permitting efficient coevolution of fungal pathogen(s) with their host(s). The ascomycete *Fusarium graminearum* is a devastating pathogen of cereal crops, and can contaminate food and feed with harmful mycotoxins. Previous studies suggest a high-adaptive potential of this pathogen, illustrated by an increase of pathogenicity and resistance to fungicides. In this study, we provide the first detailed picture of the crossovers events occurring during meiosis and discuss the role of recombination may play for pathogen evolution. An experimental recombinant population (n=88) was created and genotyped using 1,306 polymorphic markers obtained from Restriction site Associated DNA sequencing (RAD-seq) and aligned to the reference genome. The construction of a high-density linkage map, anchoring 99% of the total length of the reference genome, allowed the identification of 1,451 putative crossovers, positioned at a median resolution of 24 kilobases. The majority of crossovers (87.2 %) occurred in a relatively small portion of the genome (30 %). All chromosomes demonstrated recombination-active sections which had a near 15-fold higher crossover rate than non-active recombinant ones. Recombination rate had a strong positive correlation with nucleotide diversity, and recombinant active regions were enriched for genes with a putative role in host-pathogen interaction, as well as putative diversifying genes. Our results confirm preliminary analysis observed in other *F. graminearum* strains and suggest a conserved 'two-speed' recombination landscape. The consequences on the evolutionary potential of this major fungal pathogen are also discussed.

Introduction

Fusarium graminearum sensu stricto is one of the main causal agent of *Fusarium* Head Blight (FHB), a disease of cereal crops that constitutes a limiting factor for global production (Trail, 2009). The most damaging aspect of FHB infection is contamination of grains with stable and harmful mycotoxins such as deoxynivalenol (DON), whose presence in food and feed are widely regulated throughout the word (Waskiewicz and Golinski, 2013). Therefore, research targeting improved understanding of this pathogen and its control are a critical to food security.

In addition to homothallic reproduction, the genetic diversity observed between field isolates suggests that *F. graminearum* outcross frequently (Chen and Zhou, 2009; Liang *et al.*, 2014; Talas and McDonald, 2015a). Fungal pathogens that exhibit mixed reproduction can evolve rapidly, thereby endangering the efficiency and the durability of control strategies (McDonald and Linde, 2002; Pariaud *et al.*, 2009). Concerning *F. graminearum*, a shift towards more aggressive endogenic populations has been reported (Ward *et al.*, 2008), as well as the emergence of isolates resistant to fungicide (Chen and Zhou, 2009; Talas and McDonald, 2015b). Furthermore, experimental studies have revealed more aggressive strains following sexual outcrossing (Cumagun and Miedaner, 2004, Voss *et al.*, 2010), providing a role of sexual reproduction and recombination in maintaining or increasing aggressiveness. A better characterization of recombination in *F. graminearum* is needed to understand pathogen evolution.

F. graminearum is haploid for most of its life cycle, but meiosis can occur in the fruiting body (perithecium) formed after fusion of two haploid hyphae (Trail, 2009). Meiosis is a highly-conserved mechanism in eukaryotic genomes, of which double-strand breaks are formed between homologous chromosomes, ensuring their proper transmission and leading to either crossover events or non-crossover events (Mezard *et al.*, 2015). Both events can have direct mutagenic effects due to gene conversion (Mezard *et al.*, 2015). However, only crossovers will break parental haplotypes, limiting hitchhiking of large chromosomal segments during selection (Charlesworth and Campos, 2014). Crossover rate has been

shown to be highly variable along eukaryotic genomes (Bensasson, 2011; Bhakta *et al.*, 2015; Brachet *et al.*, 2012; Croll *et al.*, 2015; Mezard, 2006; Petes, 2001; Sonnenberg *et al.*, 2016; Tsai *et al.*, 2016; Yelina *et al.*, 2015). Furthermore, recent insight from several fungal plant pathogen genomes revealed a bipartite distribution of recombination activity, diversity, and gene function, often referred to as the "two-speed" genome hypothesis (Croll and McDonald, 2012; Dong *et al.*, 2015; Raffaele *et al.*, 2010).

In *F. graminearum*, the first draft of the genome assembly revealed a relatively condensed genome (36 Mb), of which 13,718 genes were annotated using an automated approach (Cuomo *et al.*, 2007; Wong *et al.*, 2011) while genome-mining analysis suggested a significant number of effectors as secreted proteins or secondary metabolites (Brown *et al.*, 2012; Sieber *et al.*, 2014). Alignment of the reference genome with a linkage map suggested an increase of recombination rate within telomeric / subtelomeric regions, in addition to interstitial regions (Cuomo *et al.*, 2007; Gale *et al.*, 2005). However, since both the linkage map and the genome assembly were incomplete, the interpretation of these results is limited. Strikingly, the genes hypothesized to be induced in host-pathogen interactions were more polymorphic and often located in regions of high recombination (Cuomo *et al.*, 2007). Despite the recent revision and improvement of the reference genome assembly (38 Mb, 14,164 protein-coding genes, King *et al.*, 2015), the linkage maps currently available lack the required resolution to provide better insight into the patterns of recombination across the genome (Gale *et al.*, 2005; Lee *et al.*, 2008). Additionally, questions arise about the organization of polymorphism in different genetic backgrounds, and the role of recombination in the distribution of polymorphisms. Recently, sequencing-based genotyping strategies have revolutionized the process of obtaining genome-wide marker data (Davey *et al.*, 2011). Of these techniques, restriction site associated DNA (RAD) sequencing has been widely employed for generation of high density linkage maps for several species (e.g. Baird *et al.*, 2008; Davey *et al.*, 2013; Gonen *et al.*, 2014; Lendenmann *et al.*, 2014; Palaiokostas *et al.*, 2013).

Our working hypothesis was that we would detect regions with high and low levels of recombination consistent with "two-speed" genome architecture in *F. graminearum*. In order to test such hypothesis, we

assess the distribution of meiotic recombination events in *F. graminearum* by constructing an accurate, high resolution genetic map based on RAD sequencing data from a progeny set of 88 strains. Finally, these results give new clues about the role of recombination for the evolution of this pathogen.

Results

Strains and genotyping

The parental strains used for this analysis, namely INRA-156 and INRA-171, were isolated from wheat in France. We resequenced their genomes to help with downstream analysis, and to enable an accurate reference-based RAD sequencing approach to genotyping. In total, 63,486 single nucleotide polymorphisms (SNPs) were discovered. Using parental genomes, we simulated *Pst*I enzyme digestion of the INRA-156 and INRA-171 genomes, which predicted 12,610 and 12,634 fragments with a mean size of 3,016 base pairs (bp) and 3,010 bp respectively. The large majority of cutting sites were common between the two genomes (12,489). Cutting site distribution for *Pst*I was predicted to be random (KS test, *p*-value > 0.01) avoiding introducing subsequent bias (Figure 1, track B), suggesting that the use of *Pst*I was appropriate.

Digestion of genomic DNA from the 88 recombinant progeny and from the two parental strains using the *Pst*I enzyme was followed by restriction site associated DNA (RAD-seq) library preparation and Illumina paired-end sequencing. A total of 401,726,418 paired end reads of 125 bp were produced, resulting in a total of 50.2 Gbp of sequence data. Filtering and demultiplexing resulted in a variable number of reads assigned per strain (ranging from 308,147 – 10,818,740), the majority of which were successfully aligned with the reference genome (97%). A catalogue of sequenced loci was constructed, recovering 17% of the total length of the reference genome. Strain specific sequences matching to the catalogue resulted in the identification of 1,866 polymorphic loci of which 1,306 passed the quality control requirements (Figure 1, track D). Segregation profiles of 31 randomly chosen RAD loci SNPs were matched to corresponding profiles obtained from cleaved amplified polymorphic sequences (CAPS) assays. Only 15 mismatches

were observed out of the 2,714 combinations with known genotypes, giving an overall correspondence of 99.4% (data not shown).

The dataset of markers used for downstream analysis was composed of 1,306 RAD markers, 21 markers genotyped during the validation of recombinant strain isolation, together with three additional markers named KSNP100, KSNP101 and KSNP102 (Supplemental file 1). Chromosome I and chromosome II were underrepresented (chi-square test, p-value < 0.001) and overrepresented (chi-square test, p-value < 0.001) in markers respectively, while no significant tendency were observed for the two other chromosomes. Distribution of markers along chromosomes was not random (Figure 1 track D, p-value < 0.01), with maximal distance between pairs of markers of 498.8kb (chromosome I at the position 4.0Mb to 4.5Mb). Median physical distance between markers was 12.9 kilobases (kb) ranging from 11.6 for Chrom II to 15.1 for Chrom IV (Table 1). Marker density was highest in subtelomeric and interstitial regions within chromosomes (Figure 1, track D), and correlated with the density of SNPs detected between parental genomes (Figure 1, track C, Rho=0.76, p-value<2.2E-16). An exception to this pattern was observed at the end of chromosome IV (~1.3 megabases), where highly repetitive rRNA-encoding DNA content resulted in difficulty in read alignment and subsequent variant calling. Due to the repetitive nature of the DNA in this region, there were very few informative polymorphic markers, despite an apparent abundance of *Pst*I restriction sites (Figure 1). For the remainder of the genome, the pattern of polymorphic marker distribution along the chromosomes is likely to reflect polymorphism rate rather than restriction site frequency, due to the random distribution of *Pst*I sites.

Segregation analysis, linkage map construction and alignment to the reference genome

Only five markers, sparsely located on the genome were found to exhibit segregation distortion (p-value < 0.01, Supplemental file 2 Table S1). Regarding the segregation pattern of these markers, we assumed that the observed bias of segregation could be reasonably attributed to missing data or genotyping errors. In contrast to the segregation of chromosomal markers, segregation analysis of mitochondrial markers and

KSNP102 marker (Supplemental file 1) revealed uniparental inheritance from INRA-156Δ*mat* strain of mitochondria and of HG970330 sequence respectively.

Investigating marker information across the progeny, 483 different profiles of segregations were identified. Only one representative marker per profile was used to construct the framework linkage map (n=483; Figure 1, Table 1). Four linkage groups, named "LG-1", "LG2", "LG-3" and "LG-4" were constructed (LOD threshold = 6), corresponding respectively to chromosomes I, II, III and IV described in the reference genome assembly (version 4.0). Markers were then ordered and genetic distances were calculated using Kosambi function (Table 1). Alignment of the linkage map to the reference genome revealed a remarkable collinearity (Figure 2, Supplemental file 1C). Only thirteen pairs of markers exhibited inverted order out of a possible 479 pairs of successive markers (2.7%). Manual investigation of these pairs revealed that the order of seven could be inverted and resulted from incertitude due to the map resolution. The six other pairs remained inverted, and may reflect errors in the linkage map or reference genome assembly order (Figure 2, black stars). The final map length was 1,497.1 cM with an average genetic distance between markers of 3.1 cM (Table 1).

Marker orders and distances given by this linkage map were then used to add the 847 co-segregating markers (those showing similar patterns of segregation compared to the representative markers), anchoring a total of 99.0% of the markers to the reference genome (Table 1). By doing so, one additional pair of inverted markers was detected at the end of the chromosome four (Supplemental file 1C). The markers KSNP100 and KSNP101, designed to align the supercontig 3.31 and supercontig 3.15 of the reference genome FGDG v3.1 have been successfully anchored to the chromosome I and II respectively (Figure 2), and this is in agreement with location proposed in RRes V4.0 assembly (Supplemental file 2 Table S2). Similarly, the RADseq markers C4p8034708 to C4p9403033, constituting a single recombination block, aligned the end of the chromosome IV previously proposed in the RRes V4.0 assembly (Figure 2, Supplemental file 2 Table S2).

Recombination landscape

By using the segregation information of the 1,330 markers ordered on the linkage map, 1,451 putative crossovers were mapped, within intervals of a median length of 24 kb. The average recombination rate across the entire genome was high at 39.4 cM/Mb (+/- 12.1 cM/Mb, Table 1). For each strain, 4.4 crossovers per chromosome were detected, giving an average of one crossover every 2.4 Mb (Table 1). However, recombination rate was variable between chromosomes and ranged between 30.7 cM/Mb for chromosome IV up to 58.1 cM/Mb for chromosome II (Table 1). Due to the limited number of chromosomes, the correlation between recombination rate and chromosome length could not be statistically tested, but no obvious pattern was evident.

A high level of variation in recombination rate within chromosomes was typically observed, as seen in Figure 3 that represents the alignment of the linkage map (y-axis) with the physical map (x-axis). Recombination-active sections, corresponding to regions with positive slope in the curve and with at least two-fold more recombination than the genome-wide average of 78.8 cM/Mb, and recombination deserts, corresponding to flat regions in the curve, could be identified for each chromosome. Twelve chromosomal segments greater than 0.5 Mb in length were identified as recombination active (Supplemental file 2, Table S3). Nine recombination hotspots, *i.e.*, with more than four crossovers in a 20 kb region, were detected on all chromosomes (supplemental file 2, Table S4). Isolated recombination hotspots did not always result in recombination-active sections, as illustrated by the hotspot on chromosome III at 3.4 Mb that was not associated with any recombination-active section (Figure 4). The recombination-active sections cover 30% of the physical genome, 56% of the total number of markers, and 87% of the length of the linkage map. Chromosome I contained two distal recombinant-active sections, and two proximal and central sections, each flanked by a recombination desert of 1 Mb in size. Chromosome II contained three recombinant active sections, with the intermediate one alone encompassing more than one half of recombination activity recorded in the entire chromosome. Chromosome III contained two recombinant active regions spanning more than half of the linkage group. Chromosome IV contained three recombinant-active sections, but in contrast to other chromosomes, one

subtelomeric region contained a non-recombinant chromosomal segment, corresponding to rRNA rich encoding region (Figure 3, Figure 4 track A in dark grey). Marker density was greater in active sections and varied by a 2.4 fold factor in average between sections. Average recombination rate was drastically different between non-active and active sections and varied overall by a 15.3 fold factor in average (Figure 5A). Recombination rate in the defined recombination-active sections ranged from 103.9 – 175.8 cM / Mb (Figure 5A, Supplemental file 2 Table S3), while the recombinant rate of recombination 'deserts' ranged from 3.7 to 25.0 cM/Mb (Figure 5A). The total physical length of recombinant-active sections per chromosome was positively correlated with overall chromosome recombination rate (Figure 5B).

Functional and sequence enrichment analysis of highly recombinant regions

Overall, crossover density was positively correlated with polymorphism rate (measured in SNPs/kb) along the genome (Figure 4, track B, Rho=0.67 *p*-value < 2.20E-16). Crossover density was also positively correlated with gene density along the genome (Rho=0.50, *p*-value < 2.20E-16), and negatively with GC content (Rho= -0.56, *p*-value < 2.20E-16). No correlation was observed between non-synonymous / synonymous ratio and crossover count, as calculated in 100 kb bins. However, the majority of genes showing an excess of mutation with non-synonymous effects identified in this analysis (92 of the 121 genes identified), and supposed to represent genes under diversifying selection, were located into recombinant active sections (Figure 4 track G).

Several distinct local regions show high levels of polymorphism while no recombination have been detected (Figure 4). Four of them are located within the predicted centromeres of the chromosomes (Figure 4, red squares on track A and track B). Three others regions, dispersed throughout the genome, showed similar patterns (Figure 4 track B). As previously reported, the regions located at the predicted centromeres positions always show large decreases in GC content, and this feature was not observed for these other three regions (Supplemental file 2 Table S5).

The 12 recombinant-active regions contained a total of 4,947 genes, representing 35% of the total number of protein encoding genes annotated in the reference genome (Supplemental file 3A). Gene ontology analysis of these genes revealed several enriched categories (Supplemental file 3B). Highest significant enrichment was recorded for amino-acid and transmembrane transport, oxidation reduction and carbohydrate metabolic processes, as well as the regulation of several cellular processes as transcription or nitrogen compound metabolism (1.97-fold - 1.27-fold, Supplemental file 3B). At the other end of the spectrum, recombinant-desert sections were enriched for gene categories arguably associated with basal mechanism, like localization and protein transport and metabolism or translation (Supplemental file 3B). Nonetheless, it is worth noting that 50.4% percent and 42.8 % percent of the protein coding genes located in active and desert section, respectively, have no predicted GO code.

Following the general gene ontology approach described above, a more specific enrichment analysis was performed using specific datasets of *F. graminearum* retrieved from the literature. For example, genes predicted to encode for secreted proteins, and suggested to be putative effectors, were enriched by 2 fold in recombinant active regions (p-value < 0.001, Figure 4 track E and Supplemental file 3C), as were genes predicted to act in secondary metabolite biosynthesis (Figure 4 track F, 1.4 fold, p-value < 0.001), or those previously reported to show host-specificity of expression (2.0 fold, p-value < 0.001, Figure 4 track D and Supplemental file 3C). In addition, genes previously showed to be expressed non-specifically during the infection of a panel of hosts were over-represented in non-recombinant section, and under-represented by 1.5 fold in recombinant active regions (p-value < 0.001, Figure 4 track C and Supplemental file 3C).

To go further, motif enrichment analysis of genes located in recombinant-active sections (including 500 bp upstream and downstream sequences) revealed a significant overrepresentation of motifs similar to C2H2 zing finger factors of *S. cerevisiae* (p-value < 1E-14), as well as motifs similar to High Mobility Group of *Mus musculus* (Supplemental file 2 table S6, p-value < 1E-13).

Discussion:

In this study we estimated recombination activity, and its distribution across the genome, of *F. graminearum* by using the first high density linkage map of the species based on RAD sequencing. The linkage map is almost fully integrated with the reference genome sequence (99%). It also improves the resolution of previously published genetic map of *Fusarium graminearum* by six fold (Gale *et al.*, 2005; Lee *et al.*, 2008), allowing the first thorough characterization of the recombination landscape of the species.

Crossover mapping reveals chromosome-specific landscape of recombination.

Recombination rate and its distribution is a key component of genome biology, and can vary tremendously across organisms. In sexually reproducing fungi, recombination rate was reported to vary from ~11cM / Mb in the edible mushroom *Agaricus bisporus var. bisporus* (Sonnenberg *et al.*, 2016), up to ~600 cM / Mb in *Saccharomyces cerevisiae* (Mancera *et al.*, 2008). The recombination rate estimates in this analysis for *F. graminearum* (~39 cM / Mb) is substantially lower overall than *S. cerevisiae*, and other pathogenic fungi like the causal agent of the wheat Septoria Tritici Blotch, *Zymoseptoria tritici* (130 cM / Mb, Lendenmann *et al.*, 2014). However, this recombination rate is consistent with a previously reported estimate for *F. graminearum* (~34 cM / Mb, Gale *et al.*, 2005), and may be higher due to the increased power to detect crossover using high resolution genomic tools (Sonnenberg *et al.*, 2016). Overall it suggests that *F. graminearum* does not have a particularly high genome-wide recombination rate in comparison to other pathogenic fungi. Furthermore, genome-wide average recombination rates do not reflect the variation observed along chromosomes.

In many eukaryotic species, an increase in recombination rate is observed in subtelomeric regions, and a decrease near centromeres (Bhakta *et al.*, 2015; Croll and McDonald, 2012; Cuomo *et al.*, 2007; Jensen-Seaman *et al.*, 2004; Limborg *et al.*, 2016; Mancera *et al.*, 2008; Sonnenberg *et al.*, 2016; Tsai *et al.*, 2016). As highlighted previously (Cuomo *et al.*, 2007; Gale *et al.*, 2005), *F. graminearum* is no exception to this rule. However, additional regions of the genome with high recombination rate have also

been described in interstitial regions and corresponding to previously suggested ancestral chromosomal fusions sites (Cuomo *et al.*, 2007; Ma *et al.*, 2010). Markers were not randomly distributed in the genome and we suggest this result to arise from the non-random distribution of polymorphism in the genome. The variation in marker density along the genome may have affected the accuracy on CO detection in some regions compared to others (Posada *et al.,* 2002). However, the difference in magnitude between recombination rate variation and marker density variation along the genome supports the existence of true biological explanations rather than experimental bias. The recombination patterns we identified in the present study are strikingly consistent with previous reports that used different strains (Cuomo *et al.*, 2007; Gale *et al.*, 2005), albeit at a higher resolution, suggesting foundational control of recombination in *F. graminearum*. The downstream analysis discussed below provides some insight into potential explanations of this phenomenon.

This high density linkage map was also used to test the latest version of the *F. graminearum* reference genome assembly, which is based solely on short read alignment (King *et al.*, 2015). The supercontigs not positioned in the genome reference FGDB v3.1 (Cuomo *et al.*, 2007; Wong *et al.*, 2011) that were assembled in version RRES v4.0, were consistent with our linkage map assignments. The last remaining unassigned sequence contig (HG970330) in RRES v4.0 was found to show cytoplasmic inheritance, in line with the hypothesis of phage DNA given by King *et al.* (2015). It is surprising that these DNA sequence conserved in non related strains even though the four genes encoded on this sequence (King *et al.*, 2015) may have important cellular function(s).

The predicted positions of centromeres proposed by King *et al.* (2015) were also consistent with the typical recombination pattern of centromeres identified in the current study. Centromeric regions typically shows adenosine and thymine rich sequences, have high DNA polymorphism whereas recombination is suppressed due to physical constraints (Bensasson *et al.*, 2008; Henikoff *et al.*, 2001; King *et al.* 2015). Interestingly, other genomic positions demonstrate similar characteristics according to polymorphism and recombination rate, and could correspond to ancestral centromeres following

chromosome fusions. Nevertheless, the base composition of these putative centromeres were not enriched in adenosine and thymine, suggesting either that they have lost their functions or that the patterns observed for these regions arise from different reasons. The DNA sequences of these regions (Supplemental file 5) may help to identify their roles and their origins.

Characterization of recombinant-active genome regions

Overall, the recombination landscape of *F. graminearum* and its close relative *F. pseudograminearum* (Gardiner *et al.,* 2016) is rather unique amongst fungal species studied to date. There are clearly defined peripheral and central genomic regions where the recombination activity differs by a ~15-fold factor in comparison to recombinant-desert regions. The fact that chromosomes contain specific recombinant-active regions in interstitial DNA supports the theory of distinct chromosome fusion events (Ma *et al.*, 2010), that have retained their recombination characteristics, possibly related to conserved molecular mechanisms.

Tremendous advances have been made in model species to understand the molecular mechanisms controlling meiotic recombination, including the important role of epigenetics (Brachet *et al.*, 2012; Galazka and Freitag, 2014; Mezard *et al.*, 2015). For example, euchromatin seems to favor crossover formation compared to heterochromatin. However, a paradox remains in *F. graminearum* as the epigenetic mark associated with "recombinophobic" chromatin in most organisms is enriched in recombination-active regions (Connolly *et al.*, 2013).

Variation in recombination rate can also be attributed to the action of several genes, or specific sequences, for which absence or presence can control recombination rate locally or globally on a genome (Catcheside, 1981, Mercier *et al.*, 2015, Yeadon *et al*., 2002, Yeadon *et al*., 2004, Wahls and Davidson, 2010). An example is the case of the mating type genes; associated in some species to a suppression of the recombination in their vicinity whereas recombination seems to be induced nearby in other species (Idnurm *et al.*, 2015). In this analysis, the *Mat* locus of *F. graminearum* (at position 3.0 Mb of the

chromosome II), was found in a region where the recombination was suppressed hundreds of kilobases away. At a broader scale, consensus sequences are known to be linked to recombination hotspots in several eukaryotes (Wahls and Davidson, 2010), as for example for the M26 motif (5'-ATGACTG-3'). Preliminary results made using our data suggest that the presence of such motifs is also linked with the global recombination activity observed herein for *F. graminearum* (data not shown). Furthermore, an interesting perspective would be to identify homologous proteins of model species known to be implicated in during double strand break formation or repair (see Mercier *et al.*, 2015 for a review) in *F. graminearum* and test their role in the organization of the recombination activity. For example, the Spo11 protein (likely to correspond to FGRRES_05949) implicated in double strand break formation, or the FANCM-like protein (likely to correspond to FGRRES_17603) involved in the repair of DSB in NCO rather than in CO (Girard *et al.*, 2015; Lorenz *et al.*, 2012) are interesting targets.

The in-depth recombination pattern proposed by our work marks an important milestone in the study of recombination in *F. graminearum* and open great perspectives to study its control in this pathogenic species.

Recombinant-active sections seems to be linked to several crossover hotspots

Relatively small genomic regions (1 to 5 kb) with high crossover rate have been identified in a wide range of organisms (mammals, plants, yeast), and are commonly referred to as "hotspots" (Mancera *et al.*, 2008; Mezard, 2006; Mezard *et al.*, 2015; Paigen and Petkov, 2010). Hotspots often are located in promoters of genes, leading to the hypothesis that they are associated with chromatin accessibility (Brachet *et al.*, 2012; Comeron *et al.*, 2012;Goodstadt, 2011). High recombination levels can be defined in two ways; tightly defined smaller regions corresponding to the precise length of crossover hotspots, and a broader scale genomic region corresponding to recombinant-active sections (Comeron *et al.*, 2012; Duret and Arndt, 2008; Myers *et al.*, 2005, Simchen et Stamberg, 1969), as analyzed in the current study. Enrichment of motifs similar to yeast C2H2 zinc finger, or to High Mobility Group motifs in genes located in

recombinant active regions is interesting because these motifs have previously been implicated in hotspot formation (Bergeron *et al.*, 2005; Baudat, 2010; Goodstadt, 2011; Panday *et al.*, 2016) and could be directly correlated to hotspot presence in *F. graminearum*. . We found such limited hotspots in the *F. graminearum* genome, and the frequency of these hotspots may help define larger recombination-active regions of the genome. In *Z. tritici*, it has been demonstrated that hotspots are not always consistent between crosses (Croll *et al.*, 2015). Although the data in the current study do not exclude the possibility of transient hotspots in *F. graminearum*, the general conservation of the recombination pattern across multiple genetic backgrounds (Cuomo *et al*., 2007) suggests that their locations are conserved along the genome, as observed in human chromosomes (Myers *et al.*, 2005).

Potential role of recombination landscape in pathogen evolution

As we observed and as previously reported (Cuomo *et al.*, 2007), the distribution of recombination events and polymorphisms are strikingly similar across several different *F. graminearum* genomes, a common feature of other eukaryotic genomes (Charlesworth and Campos, 2014; Manzano-Winkler *et al.*, 2013; Noor, 2008; Roselius *et al.*, 2005; Spencer *et al.*, 2006). Sexual recombination with different partners, and suggested to occur at high frequency in *F. graminearum* population (Talas and McDonald, 2015a), can play a role in evolution by increasing genotypic diversity and enabling selection of favorable alleles and haplotypes in selective sweeps (Goddard *et al.*, 2005).

Linkage disequilibrium resulting from the lack of recombination in recombination deserts, coupled with the presence of genes under positive and purifying selection should reduce nucleotide diversity over time via selective sweeps (Smith et Haigh, 1974). In *F. graminearum*, genes expressed independently to the host infected, which may correspond to conserved biological functions (Harris et al., 2016), are over-represented in regions with low observed levels of recombination, while genes expressed in a host-specific manner are over-represented in regions with high observed levels of recombination. The diversifying selection acting on host-specific effectors (Sperschneider *et al.*, 2015) such as secreted proteins or genes

implicated in secondary metabolite production (Brown *et al.*, 2012; Harris *et al.*, 2016; King *et al.*, 2015; Sieber *et al.*, 2014) is probably made efficient by the frequent break up and reshuffle of haplotypes in these regions and favor genotypic diversity.

Under the hypothesis that recombination is mutagenic during DNA repair, as demonstrated in yeast (Strathern *et al.*, 1995), the higher rate of recombination observed in active sections of *F. graminearum* genome may create genetic diversity. This latter point would thus make both the heterothallic and the homothallic reproduction an additional source of diversity and a driver for evolution.

Overall, the distribution and characterization of observed recombination events in *F. graminearum* are consistent with the emerging concept of a bipartite architecture of genome evolution in pathogenic fungi, also referred as "two speed" genome. Under this concept, genes that are critical to host-pathogen interaction cluster in genomic regions associated with high recombination, to facilitate a more rapid evolutionary response (Croll *et al.*, 2015; Dong *et al.*, 2015). However, the recombination pattern in *F. graminearum* differs from other fungal pathogens in at least two aspects: (i) *F. graminearum* has unusual chromosome architecture, and (ii) the epigenetic marks associated with recombination activity are not always located in areas where they are predicted to be. The uniqueness of the *F. graminearum* recombination patterns and genome organization make this pathogen a significant exception to some of the emerging patterns of fungal genome organization, and suggests that genome organization is a dynamic process that remains in flux rather than a static arrangement. Overall, these results shed light on the high potential of adaptation inherent to the recombination landscape of this pathogen and alert about the risk of apparition of more aggressive populations.

Experimental procedures

Progeny construction and culture conditions:

The INRA-156 and INRA-171 strains were isolated from wheat in 2001 and 2002 in different fields of Center and South-West of France respectively. Strains were characterized as *Fusarium graminearum sensu stricto* and are both pathogenic and toxinogenic on wheat. Eighty-eight (88) recombinant strains were produced from a cross between polymorphic INRA-156*Δmat* strain and INRA-171 strain. Recombinant strains were further validated using 21 targeted marker assays (see "Targeted marker genotyping" section and Supplemental file 1 & 5). Potato dextrose agar (PDA, Difco-France) was used throughout vegetative growth. INRA-156Δ*mat* was obtained from INRA-156 strain by replacing the *mat1-2-1* coding sequence (FGREES_08893) by a hygromycin resistance cassette using split marker method (Goswami, 2012, Supplemental file 4). The crossing procedure was adapted from Lee *et al.*, 2003 and Leslie et Summerell, 2006, except for incubation that has been conducted under continuous white light (Osram T8 L 36W 840 G13 Lumilux). The plate was incubated at 25°C under continuous white light, until perithecia reached maturity (Cavinder *et al*., 2012). Visible cirrhi were collected in sterile water, spread and incubated on PDA plates. Single germinating spore were isolated twice as previously described in Leslie et Summerell, 2006.

Genomic resources:

The *F. graminearum* genome version RRes V4.0 (King *et al.*, 2015) used in the study is available at EMBL-EBI (HG970331, HG970332, HG970333, HG970334, HG970335). Genes predicted to code for the secreted proteins of *F. graminearum* were retrieved from King *et al*., (2015). Genes previously described as expressed in wheat, barley and/or maize were retrieved from Harris *et al.,* (2016) and the genes predicted to belong to secondary metabolite pathway clusters were retrieved from Sieber *et al*., (2014).

Genomic DNA extraction:

Genomic DNA was extracted from lyophilized mycelium previously grown on potato dextrose agar (39 g/l, Difco). Mycelia were lysed in a buffer containing 100 mM Tris-Hcl (pH 9.0), 10 mM EDTA, 1%

sarkosyl and 200 µg/mL proteinase K for 2 h at 65 °C. After centrifugation (10 min at 10,000 g), the supernatant was extracted successively with phenol, phenol: chloroform (50:50) and finally chloroform. Nucleic acids were precipitated with cold ammonium acetate (3M) and isopropanol, washed in 70% ethanol and dissolved in 100 µL nuclease free water.

Whole genome sequencing of parental strains and analysis:

Whole nuclear DNA from the parental isolates were sequenced by the MGX platform in Montpellier, France (http://www.mgx.cnrs.fr/) using the Illumina sequencing technology (HiSeq™ Sequencing Systems). The reads were filtered and trimmed using Prinseq software (Schmieder and Edwards, 2011). They were then aligned to the reference genome RRes V4.0 (King *et al.*, 2015) using BWA (v 0.7.8) and the BWA-MEM algorithm with standard parameters, and a seed size of 15 nucleotides (Li and Durbin, 2009). SNP calling was performed using GATK (v 2.4) and the Unified Genotyper walker in haploïd mode (DePristo *et al.*, 2011). Parental consensus sequences were constructed using VcfToFasta tool, and by correcting the reference genome with variants identified in each parental genome. *In silico* digestion of the genomes by *Pst*I enzyme was conducted using EMBOSS and the "Restrict" tool. Genes showing an excess of mutations were identified and defined as exhibiting more than 75% of non-synonymous mutations compared to total number of mutation into genic sequence (upper 3rd quartile of genome wide distribution) and at least 4 genic mutations (genome wide median mutation number per gene x 2).

RAD-seq library preparation and sequencing

Library and sequencing was prepared and conducted by the MGX platform team in Montpellier, France (http://www.mgx.cnrs.fr). The libraries were prepared according to Baird *et al.* (2008) using the *Pst*I restriction enzyme. The main modification was the use of Ampure XP beads for the different purification steps. A detailed version of RAD-seq procedure is available in Supporting Materials. Sequence data are retrievable from GenBank database under SRA accession SRP083578.

RAD-seq SNP discovery and genotyping analysis

The quality of the 125-nt long paired-end reads was analyzed using FastQC v0.11.2. Reads were demultiplexed according to barcode sequences using 'process_radtags' program from Stacks software pipeline v1.32 with the following parameters: *Pst*I enzyme cutting site recognition, removal of reads with at least one uncalled base and/or an average quality score below the phred score of 20. For each strain, reads were then mapped on the reference genome RRes V4.0 (King *et al*., 2015) using Bowtie2 v0.12.9 using default parameters. SAM files were then sorted and transformed to BAM files using Samtools v1.1 (Li *et al*., 2009). The stacks software (Catchen *et al.*, 2011) was used all along to identify SNP and InDel markers. The ref_map.pl program was used to i) compare both parental BAM files and the 88 BAM files from the progeny in order to build RAD loci and call SNPs, ii) create a catalog of all loci and iii) match each sample against the catalog. The minimum depth of coverage to call a stack was 3, one mismatch was allowed between loci when building the catalog. Markers were retained if they were bi-allelic, contained up to 10 SNPs compared to the consensus sequences, and at least 80% of the progeny were genotyped.

Targeted marker genotyping

Single Nucleotide Polymorphism (SNP) derived markers genotyped using either Cleaved Amplified Polymorphic Sequences (CAPS) or Kompetitive Allele Specific PCR (KASP) techniques have been designed from the whole genome polymorphism information between the two parental sequences. Microsatellite (Simple Sequence Repeat SSR) markers have been retrieved from literature (Brygoo and Gautier, 2007; Giraud *et al.*, 2002; Naef *et al.*, 2006; Naef and Défago, 2006; Vogelgsang *et al.*, 2009). Ten SSR and 11 CAPS markers were used to confirm the recombinant progeny. Three KASP markers were designed to align supercontig 3.31, supercontig 3.15 and supercontig 3.12 respectively. These sequences corresponded to supercontigs that were not anchored during initial assembly (Cuomo et *al.,* 2007). The first two supercontigs have been anchored in the version RRes V4.0. Supercontig 3.12 (HG970330) remains unanchored. Details about primers and experiment conditions are available in Supplemental File 6.

Genetic map construction:

The linkage map was constructed using R/qtl (Broman *et al.*, 2003). Firstly, markers exhibiting redundant segregation patterns in the population were set aside from the mapping procedure. Linkage groups were formed using a maximum recombination fraction of 0.35 and a decimal logarithm of odd (LOD) score threshold of 6. Markers were ordered and genetic distance was calculated using the Kosambi function. Groups of co-segregating markers were repositioned manually at marker position (the one used for linkage map construction) and following reference genome order. Genotyping errors were investigated using the calc.errorlod function of R/qtl and the identified genotypes were replaced by missing data. Inversions were manually investigated. When the likelyhoods were similar for the two alternative orders, the physical positions were preferred.

Alignment of genetic and physical maps and analysis of recombination

The linkage map was aligned on the reference genome (RRES v4.0). For RAD-tags containing several genetic variants, only the position of the first variant was considered. The ArkMap software was used to construct the illustration showing the alignment of the linkage map to the reference genome (http://www.bioinformatics.roslin.ed.ac.uk/arkmap/). The recombination rate of overall chromosome, or recombinant-active and recombinant desert sections, were calculated by dividing linkage group size by chromosome or section size. Detection of crossover was performed manually using inheritance of markers along the chromosome according to the linkage map order. The resolution of crossover position was obtained by calculating the median size spanning two markers adjacent to the corresponding crossover. Recombinant-active sections were defined when they contained a two-fold increase in recombination rate compared to the genome-wide average, over a region larger than 0.5 Mb. Recombination hotspots were defined as the genomic loci delimitated by markers of which more than 4 crossovers were recorded and presenting an estimated recombination rate greater than a ten-fold increase of genome-wide recombination rate (> 394cM/Mb).

Statistical analysis:

The Poisson distribution was used to test the distribution pattern of predicted *Pst*I cutting site and markers site in the genome. Marker distribution analysis was carried out as described in Bhakta *et al.*, (2015) using an interval of 100 kb. Significant differences between observed and expected frequencies of the number of markers per interval were tested through Kolmogorov Smirnov tests with p-value > 0.01 suggesting that the observed frequency does not show statistical difference with the expected frequency. Enrichment of functional categories was calculated using the Gene Ontology Enrichment tools proposed online by the EuPathDB project (http://fungidb.org) using Biological ontology and InterPro predictions. Enrichments were defined for p-value < 0.001. A Chi-squared test was used to compare the observed distribution of genes located in recombinant active regions compared to the theoretical distribution under the hypothesis of a random distribution in the genome. Over and underrepresentation were defined for p-value < 0.001. Gene density, GC content and observed crossovers were calculated using different windows of 100 kb bins. Correlations were calculated using Spearman rank order test correlation and accepted for p-value < 0.001. Motif search was conducted using Homer software (Heinz et al., 2010) using the findMotifs.pl script with standard parameters.

Acknowledgements

Authors would like to acknowledge the genotoul bioinformatic platform Toulouse Midi-Pyrénées and Sigenae group for providing help along the bioinformatic analysis and storage resources (http://bioinfo.genotoul.fr/). BL received a PhD fellowship from the French Research Ministry. Collaboration between the French National Institute for Agricultural Research (INRA) and The Roslin Institute was made possible thanks to a grant delivered by the Plant Health and Environment INRA division. RDH and CP were supported by the Bioscience and Biotechnology Research Council (BBSRC) funds BB/J004235/1 and BB/J004324/1.

Baird, N.A., Etter, P.D., Atwood, T.S., Currey, M.C., Shiver, A.L., Lewis, Z.A., Selker, E.U., Cresko, W.A. and Johnson, E.A. (2008) Rapid SNP discovery and genetic mapping using sequenced RAD markers. *PLoS One* **3**, e3376.

Baudat, F., Buard, J., Grey, C., Fledel-Alon, A., Ober, C., Przeworski, M., Coop, G. et Massy, B. de (2010) PRDM9 is a major determinant of meiotic recombination hotspots in humans and mice. *Science* **327**, 836.

Bensasson, D. (2011) Evidence for a high mutation rate at rapidly evolving yeast centromeres. *Bmc Evol. Biol.* **11**.

Bensasson, D., Henikoff, S., Ahmad, K., et al. (2011) Evidence for a high mutation rate at rapidly evolving yeast centromeres. *BMC Evol. Biol.* **11**, 211.

Bergeron, S., Madathiparambil, T. and Swanson, P.C. (2005) Both high mobility group (HMG)-boxes and the acidic tail of HMGB1 regulate recombination-activating gene (RAG)-mediated recombination signal synapsis and cleavage *in vitro*. *J. Biol. Chem.* **280**, 31314–31324.

Bhakta, M.S., Jones, V.A. and Vallejos, C.E. (2015) Punctuated distribution of recombination hotspots and demarcation of pericentromeric regions in *Phaseolus vulgaris L*. *PLoS One* **10**, e0116822.

Brachet, E., Sommermeyer, V. and Borde, V. (2012) Interplay between modifications of chromatin and meiotic recombination hotspots. *Biol Cell* **104**, 51–69.

Broman, K.W., Wu, H., Sen, S. and Churchill, G.A. (2003) R/qtl: QTL mapping in experimental crosses. *Bioinformatics* **19**, 889–890.

Brown, N.A., Antoniw, J. and Hammond-Kosack, K.E. (2012) The predicted secretome of the plant pathogenic fungus *Fusarium graminearum*: a refined comparative analysis. *PLoS One* **7**, e33731.

Brygoo, Y. and Gautier, A. (2007) Molecular polymorphism of *Fusarium* strains isolated from wheat and corn ears in France Collects 2003 and 2004. (Paper presented at the conférence sur les progrès et perspectives de la recherche sur les mycotoxines de Fusarium dans les céréales. Arcachon, France)

Catchen, J.M., Amores, A., Hohenlohe, P., Cresko, W. and Postlethwait, J.H. (2011) Stacks: building and genotyping loci d*e novo* from short-read sequences. *G3 Genes, Genomes, Genet.* **1**, 171–182.

Catcheside, D.E.A. (1981) Genes in *Neurospora* that suppress recombination when they are heterozygous. *Genetics* **98**.

Cavinder, B., Sikhakolli, U., Fellows, K.M. et Trail, F. (2012) Sexual development and ascospore discharge in *Fusarium graminearum*. *J. Vis. Exp.* **61**.

Charlesworth, B. et Campos, J.L. (2014) the relations between recombination rate and patterns of molecular variation and evolution in *Drosophila*. *Annu. Rev. Genet.* **48**, 383‑403.

Chen, Y. and Zhou, M.-G. (2009) Sexual recombination of carbendazim resistance in *Fusarium graminearum* under field conditions. *Pest Manag. Sci.* **65**, 398–403.

Comeron, J.M., Ratnappan, R., Bailin, S., et al. (2012) The many landscapes of recombination in *Drosophila melanogaster* Petrov, D.A., ed. *PLoS Genet.* **8**, e1002905.

Connolly, L.R., Smith, K.M. et Freitag, M. (2013) The *Fusarium graminearum* histone H3 K27 methyltransferase KMT6 regulates development and expression of secondary metabolite gene clusters. *PLoS Genet* **9**, e1003916.

Croll, D., Lendenmann, M.H., Stewart, E. and McDonald, B.A. (2015) The impact of recombination hotspots on genome evolution of a fungal plant pathogen. *Genetics* **201**, 1213–1228.

Croll, D. and McDonald, B.A. (2012) The accessory genome as a cradle for adaptive evolution in pathogens. *PLoS Pathog* **8**, e1002608.

Cumagun, C.J.R. and Miedaner, T. (2004) Segregation for aggressiveness and deoxynivalenol production of a population of *Gibberella zeae* causing head blight of wheat. *Eur. J. Plant Pathol.* **110**, 789–799.

Cuomo, C.A., Guldener, U., Xu, J.R., et al. (2007) The *Fusarium graminearum* genome reveals a link between localized polymorphism and pathogen specialization. *Science (80-.).* **317**, 1400‑1402.

Davey, J.W., Cezard, T., Fuentes-Utrilla, P., Eland, C., Gharbi, K. and Blaxter, M.L. (2013) Special features of RAD sequencing data: implications for genotyping. *Mol. Ecol.* **22**, 3151–3164.

Davey, J.W., Hohenlohe, P.A., Etter, P.D., Boone, J.Q., Catchen, J.M. and Blaxter, M.L. (2011) Genome-wide genetic marker discovery and genotyping using next-generation sequencing. *Nat Rev Genet* **12**, 499–510.

DePristo, M.A., Banks, E., Poplin, R., et al. (2011) Additional data:A framework for variation discovery and genotyping using next-generation DNA sequencing data. *Nat Genet* **43**, 491–498.

Dong, S., Raffaele, S. and Kamoun, S. (2015) The two-speed genomes of filamentous pathogens: waltz with plants. *Curr. Opin. Genet. Dev.* **35**, 57–65.

Duret, L. and Arndt, P.F. (2008) The impact of recombination on nucleotide substitutions in the human genome Przeworski, M., ed. *PLoS Genet.* **4**, e1000071.

Galazka, J.M. and Freitag, M. (2014) Variability of chromosome structure in pathogenic fungi--of "ends and odds." *Curr Opin Microbiol* **20**, 19–26.

Gale, L.R., Bryant, J.D., Calvo, S., et al. (2005) Chromosome complement of the fungal plant pathogen *Fusarium graminearum* based on genetic and physical mapping and cytological observations. *Genetics* **171**, 985‑1001.

Gardiner, D.M., Benfield, A.H., Stiller, J., Stephen S., Aitken, K., Chunji, L. and Kazan, K. (2017) A high resolution genetic map of the wheat crown rot pathogen *Fusarium pseudograminearum* provides a near complete genome assembly. *Mol. Plant Pathol., in revision.*

Girard, C., Chelysheva, L., Choinard, S., et al. (2015) AAA-ATPase FIDGETIN-LIKE 1 and helicase FANCM antagonize meiotic crossovers by distinct mechanisms. *PLoS Genet.* **11**, e1005369.

Giraud, T., Fournier, E., Vautrin, D., Solignac, M., Vercken, E., Bakan, B. and Brygoo, Y. (2002) Isolation of eight polymorphic microsatellite loci, using an enrichment protocol, in the phytopathogenic fungus *Fusarium culmorum*. *Mol. Ecol. Notes* **2**, 121–123.

Goddard, M.R., Godfray, H.C.J. et Burt, A. (2005) Sex increases the efficacy of natural selection in experimental yeast populations. *Nature* **434**, 636‑640.

Gonen, S., Lowe, N.R., Cezard, T., Gharbi, K., Bishop, S.C. et Houston, R.D. (2014) Linkage maps of the Atlantic salmon (*Salmo salar*) genome derived from RAD sequencing. *BMC Genomics* **15**, 1‑17.

Goodstadt, C.P.P. (2011) Is the control of recombination conserved among diverse eukaryotes? *Heredity (Edinb).* **106**, 710.

Goswami, R.S. (2012) Targeted gene replacement in fungi using a split-marker approach. *Methods Mol.*

Biol. **835**, 255‐69.

Harris, L.J., Balcerzak, M., Johnston, A., Schneiderman, D. and Ouellet, T. (2016) Host-preferential *Fusarium graminearum* gene expression during infection of wheat, barley, and maize. *Fungal Biol.* **120**, 111–123.

Heinz, S., Benner, C., Spann, N., et al. (2016) Simple combinations of lineage-determining transcription factors prime cis-regulatory elements required for macrophage and B cell identities. *Mol. Cell* **38**, 576‐89.

Henikoff, S., Ahmad, K. and Malik, H.S. (2001) The centromere paradox: stable inheritance with rapidly evolving DNA. *Science (80-.).* **293**, 1098–1102.

Idnurm, A., Hood, M.E., Johannesson, H. et Giraud, T. (2015) Contrasted patterns in mating-type chromosomes in fungi: Hotspots versus coldspots of recombination. *Fungal Biol. Rev.* **29**, 220‐229.

Jensen-Seaman, M.I., Furey, T.S., Payseur, B.A., Lu, Y., Roskin, K.M., Chen, C.-F., Thomas, M.A., Haussler, D. and Jacob, H.J. (2004) Comparative recombination rates in the rat, mouse, and human genomes. *Genome Res.* **14**, 528–538.

King, R., Urban, M., Hammond-Kosack, M., Hassani-Pak, K. and Hammond-Kosack, K. (2015) The completed genome sequence of the pathogenic ascomycete fungus *Fusarium graminearum*. *BMC Genomics* **16**, 544.

Lee, J., Jurgenson, J.E., Leslie, J.F. et Bowden, R.L. (2008) Alignment of genetic and physical maps of *Gibberella zeae*. *Appl Env. Microbiol* **74**, 2349‐2359.

Lee, J., Lee, T., Lee, Y.-W., Yun, S.-H. et Turgeon, B.G. (2003) Shifting fungal reproductive mode by manipulation of mating type genes: obligatory heterothallism of *Gibberella zeae*. *Mol Microbiol* **50**, 145‐152.

Lendenmann, M.H., Croll, D., Stewart, E.L. and McDonald, B.A. (2014) Quantitative trait locus mapping of melanization in the plant pathogenic fungus *Zymoseptoria tritici*. *G3 Genes|Genomes|Genetics* **4**, 2519–2533.

Leslie, J.F. et Summerell, B.A. (2006) The *Fusarium* laboratory manual, Blackwell Pub.

Li, H. and Durbin, R. (2009) Fast and accurate short read alignment with Burrows–Wheeler transform. *Bioinformatics* **25**, 1754–1760.

Liang, J.M., Xayamongkhon, H., Broz, K., Dong, Y., McCormick, S.P., Abramova, S., Ward, T.J., Ma, Z.H. and Kistler, H.C. (2014) Temporal dynamics and population genetic structure of *Fusarium graminearum* in the upper Midwestern United States. *Fungal Genet Biol* **73**, 83–92.

Limborg, M.T., McKinney, G.J., Seeb, L.W. and Seeb, J.E. (2016) Recombination patterns reveal information about centromere location on linkage maps. *Mol. Ecol. Resour.* **16**, 655–661.

Lorenz, A., Osman, F., Sun, W., et al. (2012) The fission yeast FANCM ortholog directs non-crossover recombination during meiosis. *Science (80-.).* **336**, e299–e299.

Ma, L.-J., Does, H.C. van der, Borkovich, K.A., et al. (2010) Comparative genomics reveals mobile pathogenicity chromosomes in Fusarium. *Nature* **464**, 367–373.

Mancera, E., Bourgon, R., Brozzi, A., Huber, W. and Steinmetz, L.M. (2008) High-resolution

mapping of meiotic crossovers and non-crossovers in yeast. *Nature* **454**, 479–485.

Manzano-Winkler, B., McGaugh, S.E., Noor, M.A.F., et al. (2013) How hot are drosophila hotspots? Examining recombination rate variation and associations with nucleotide diversity, divergence, and maternal age in *Drosophila pseudoobscura* Palsson, A., ed. *PLoS One* **8**, e71582.

McDonald, B. and Linde, C. (2002) The population genetics of plant pathogens and breeding strategies for durable resistance. *Euphytica* **124**, 163–180.

Mercier, R., Mézard, C., Jenczewski, E., Macaisne, N. et Grelon, M. (2015) The Molecular Biology of Meiosis in Plants. *Annu. Rev. Plant Biol.* **66**, 297‑327.

Mezard, C. (2006) Meiotic recombination hotspots in plants. *Biochem. Soc. Trans.* **34**, 531–534.

Mezard, C., Jahns, M.T. and Grelon, M. (2015) Where to cross? New insights into the location of meiotic crossovers. *Trends Genet* **31**, 393–401.

Myers, S., Bottolo, L., Freeman, C., McVean, G. and Donnelly, P. (2005) A fine-scale map of recombination rates and hotspots across the human genome. *Science* **310**, 321–4.

Naef, A. and Défago, G. (2006) Population structure of plant-pathogenic *Fusarium* species in overwintered stalk residues from Bt-transformed and non-transformed maize crops. *Eur. J. Plant Pathol.* **116**, 129–143.

Naef, A., Senatore, M. and Défago, G. (2006) A microsatellite based method for quantification of fungi in decomposing plant material elucidates the role of *Fusarium graminearum* DON production in the saprophytic competition with *Trichoderma atroviride* in maize tissue microcosms. *FEMS Microbiol. Ecol.* **55**, 211–20.

Noor, M.A.F. (2008) Connecting recombination, nucleotide diversity and species divergence in Drosophila. *Fly (Austin).* **2**, 255–6.

Paigen, K. and Petkov, P. (2010) Mammalian recombination hot spots: properties, control and evolution. *Nat. Rev. Genet.* **11**, 221–233.

Palaiokostas, C., Bekaert, M., Khan, M.G.Q., et al. (2013) Mapping and validation of the major sex-determining region in Nile Tilapia (*Oreochromis niloticus L.*) using RAD Sequencing Orban, L., éd. *PLoS One* **8**, e68389.

Panday, A., Grove, A., Hergeth, S., et al. (2016) The high mobility group protein HMO1 functions as a linker histone in yeast. *Epigenetics Chromatin* **9**, 13.

Pariaud, B., Ravigné, V., Halkett, F., Goyeau, H., Carlier, J. and Lannou, C. (2009) Aggressiveness and its role in the adaptation of plant pathogens. *Plant Pathol.* **58**, 409–424.

Petes, T.D. (2001) Meiotic recombination hot spots and cold spots. *Nat Rev Genet* **2**, 360–369.

Posada, D., Crandall, K.A. et Holmes, E.C. (2002) Recombination in Evolutionary Genomics. *Annu. Rev. Genet.* **36**, 75‑97.

Raffaele, S., Farrer, R.A., Cano, L.M., et al. (2010) Genome evolution following host jumps in the Irish potato famine pathogen lineage. *Science* **330**, 1540–3.

Roselius, K., Stephan, W. and Städler, T. (2005) The relationship of nucleotide polymorphism,

Schmieder, R. et Edwards, R. (2011) Quality control and preprocessing of metagenomic datasets. *Bioinformatics* **27**, 863‑4.

Sieber, C.M.K., Lee, W., Wong, P., et al. (2014) The *Fusarium graminearum* genome reveals more secondary metabolite gene clusters and hints of horizontal gene transfer. *PLoS One* **9**, e110311.

Smith, J.M. et Haigh, J. (1974) The hitch-hiking effect of a favourable gene. *Genet. Res.* **23**, 23.

Sonnenberg, A.S.M., Gao, W., Lavrijssen, B., et al. (2016) A detailed analysis of the recombination landscape of the button mushroom *Agaricus bisporus* var. *bisporus*. *Fungal Genet. Biol.* **93**, 35–45.

Spencer, C.C.A., Deloukas, P., Hunt, S., Mullikin, J., Myers, S., Silverman, B., Donnelly, P., Bentley, D. and McVean, G. (2006) The influence of recombination on human genetic diversity. *PLoS Genet.* **2**, e148.

Sperschneider, J., Gardiner, D.M., Thatcher, L.F., Lyons, R., Singh, K.B., Manners, J.M. and Taylor, J.M. (2015) Genome-wide analysis in three *Fusarium* pathogens identifies rapidly evolving chromosomes and genes associated with pathogenicity. *Genome Biol. Evol.***7**, 1613-1627.

Strathern, J.N., Shafer, B.K. et McGill, C.B. (1995) DNA synthesis errors associated with double-strand-break repair. *Genetics* **140**, 965–972.

Talas, F. and McDonald, B. (2015a) Genome-wide analysis of *Fusarium graminearum* field populations reveals hotspots of recombination. *BMC Genomics* **16**, 996.

Talas, F. and McDonald, B.A. (2015b) Significant variation in sensitivity to a DMI fungicide in field populations of *Fusarium graminearum*. *Plant Pathol.* **64**, 664–670.

Trail, F. (2009) For blighted waves of grain: *Fusarium graminearum* in the postgenomics era. *Plant Physiol* **149**, 103–110.

Tsai, H.Y., Robledo, D., Lowe, N.R., Bekaert, M., Taggart, J.B., Bron, J.E. and Houston, R.D. (2016) Construction and annotation of a high density SNP linkage map of the atlantic salmon (*Salmo salar*) genome. *G3: Genes|Genomes|Genetics* **6**, 2173–2179.

Vogelgsang, S., Widmer, F., Jenny, E. and Enkerli, J. (2009) Characterisation of novel *Fusarium graminearum* microsatellite markers in different Fusarium species from various countries. *Eur. J. Plant Pathol.* **123**, 477–482.

Voss, H.-H., Bowden, R.L., Leslie, J.F. et Miedaner, T. (2010) Variation and transgression of aggressiveness among two *Gibberella zeae* crosses developed from highly aggressive parental isolates. *Phytopathology* **100**, 904‑912.

Ward, T.J., Clear, R.M., Rooney, A.P., et al. (2008) An adaptive evolutionary shift in Fusarium head blight pathogen populations is driving the rapid spread of more toxigenic *Fusarium graminearum* in North America. *Fungal Genet. Biol.* **45**, 473–484.

Waskiewicz, A. and Golinski, P. (2013) Mycotoxins in foods, feeds and their components. *Krmiva* **55**, 35–45.

Wahls, W.P. et Davidson, M.K. (2010) Discrete DNA sites regulate global distribution of meiotic recombination. *Trends Genet.* **26**, 202‑208.

Wong, P., Walter, M., Lee, W., Mannhaupt, G., Münsterkötter, M., Mewes, H.-W., Adam, G. and

Güldener, U. (2011) FGDB: revisiting the genome annotation of the plant pathogen *Fusarium graminearum*. *Nucleic Acids Res.* **39**, D637–D639.

Yeadon, P.J., Koh, L.Y., Bowring, F.J., Rasmussen, J.P. et Catcheside, D.E.A. (2002) Recombination at his-3 in Neurospora Declines Exponentially With Distance from the Initiator, cog. *Genetics* **162**.

Yeadon, P.J., Bowring, F.J. et Catcheside, D.E.A. (2004) Alleles of the Hotspot cog Are Codominant in Effect on Recombination in the his-3 Region of Neurospora. *Genetics* **167**.

Yelina, N., Diaz, P., Lambing, C. and Henderson, I.R. (2015) Epigenetic control of meiotic recombination in plants. *Sci. China-Life Sci.* **58**, 223–231.

Supporting information legends

Supplemental file 1: Dataset of markers. A) Lab markers B) RAD markers C) Alignment of the genetic map with the reference genome.

Supplemental file 2: Table S1: List of markers exhibiting non-Mendelian segregation. **Table S2:** Overview of the supercontigs anchored during RRes4.0 assembly proposal, with information concerning the marker used for anchoring these supercontigs. **Table S3:** List of the chromosomal segments classified as recombinant-active. **Table S4:** List of the hypothetical crossover hotspots identified in this analysis. **Table S5**: Positions and GC content of peaks showing typical centromeric-like patterns of recombination and polymorphisms. The regions containing the predicted positions of centromeres proposed by King *et al.*, (2015) are given in yellow. **Table S6:** Motifs significantly overrepresented in genes located in recombinant active genes (gene sequence in addition to 500 bp downstream and upstream sequence).

Supplemental file 3: Recombination and gene functions. A] All protein-coding genes described in the reference genome (RRES v4.0) with features. B] Gene ontology enrichment of recombinant-active and desert sections. C] Representation of specific gene lists within recombinant-active and desert sections

Supplemental file 4: Supporting procedures

Supplemental file 5: Fasta sequences of the putative centromeres

Supplemental file 6: Targeted markers development

Tables

Table 1: General features of genotyping procedure and linkage map construction

Figures legends:

Figure 1: Circos plot of the distribution of several genomic attributes and genotyping features along the four chromosomes of *F. graminearum.* The shaded region at the end of the chromosome IV shows the highly repetitive rRNA encoding region proposed by King *et al.* (2015). A. Representation (in Mb) of the

four chromosomes of *F. graminearum*, with the positions of the predicted centromeres in red. B) Predicted *Pst*I cutting sites based on parental sequences. C) Single nucleotide polymorphism frequency between whole genome sequences of parental strains. D) Frequency of RADseq polymorphic marker sites. E) Position of markers with non-redundant segregation profiles.

Figure 2: Alignment of the linkage map (left side) to the reference genome RRES v4.0 (right side). The dark stars and the black lines represent the six inversions remaining in the linkage map. The location of the sequence placed by King *et al.* in the assembly and anchored by the linkage map is indicated in grey.

Figure 3: Scatterplot showing the linkage map position (y-axis) and physical position (x-axis). The dotted lines delimitate recombinant-active sections (numbered with arabic numerals) from recombinant-desert sections.

Figure 4: Circos plot of the distribution of several genomic se In order to identify possible bias introduced quence features along the four chromosomes of *F. graminearum.* A. Representation of the four chromosomes of *F. graminearum* (in Mb), the dashed red rectangles delimitate the positions of the predicted centromeres. B. In red the SNP density (SNPs/kb) is calculated in windows of 100 kb bins along parental genomes. In blue, the number of CO calculated in separated windows of 100 kb bins across the progeny. The dashed red rectangular boxes locate typical patterns observed at centromere positions; dashed dark boxes locate centromere-like patterns. Recombinant-active sections are highlighted in yellow. C. Protein coding genes expressed constitutively in *all planta* conditions (Harris *et al.,* 2016). D. Protein coding genes expressed in host-specific conditions (Harris *et al.,* 2016). For C and D, gene density was calculated in 100 kb bin windows E. Location of genes predicted to code for secreted proteins (Brown *et al.,* 2012; King *et al.,* 2015). F. Location of predicted secondary metabolite clusters (Sieber *et al.,* 2014). G. Location of genes showing evidence of diversification.

Figure 5: A. Recombination rate distribution according to chromosomal section. Recombinant-active sections are given in red, and recombinant-desert sections in blue. The dashed line refers to the recombination rate threshold to be considered as recombinant-active section (2-fold increase of genome-wide recombination rate). B. The percentage of total size of chromosome allocated to recombinant-active sections is given in red, and the chromosome average recombination rate (cM/Mb) in grey.

Table 1: General features of genotyping procedure and linkage map construction

Linkage group / Chromosome	Marker number	Average marker number per 100kb	Median distance between markers (kb)	Max distance between markers (kb)	Marker used for linkage map construction*	Average spacing (cM)	Linkage group size (cM)	Chromosome size (Mbp)	Recombination rate (cM/Mb)	% anchored	Average number of CO per strain
LG-1 / Chrom I	342	2.9	11.7	499	130	3.4	435	11.76	37.0	98.0%	4.5
LG-2 / Chrom II	387	4.3	11.6	351.7	164	3.2	522.9	9.00	58.1	99.4%	5.5
LG-3 / Chrom III	278	3.6	12.8	301.1	92	2.8	250.8	7.79	32.2	99.2%	2.8
LG-4 / Chrom IV	323	3.4	15.1	398.7	97	3	288.4	9.41	30.7	99.4%	3.1
Overall	1330	3.5	12.9	499	483	3.1	1497.1	37.96	39.4	99.0%	15.9

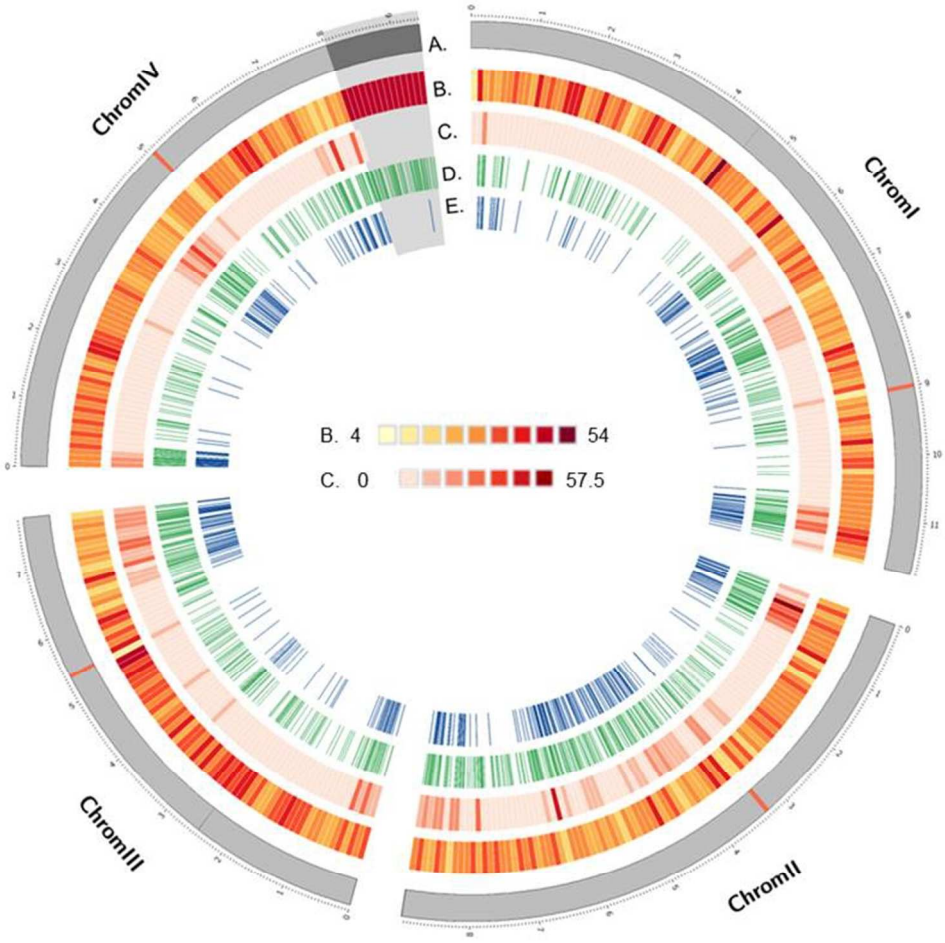

Figure 1: Circos plot of the distribution of several genomic attributes and genotyping features along the four chromosomes of F. graminearum: A. Representation (in Mb) of the four chromosomes of F. graminearum, with the positions of the predicted centromeres in red. B) Predicted PstI cutting sites based on parental sequences. C) Single nucleotide polymorphism frequency between whole genome sequences of parental strains. D) Frequency of RADseq polymorphic marker sites. E) Position of markers with non-redundant segregation profiles.

152x152mm (139 x 139 DPI)

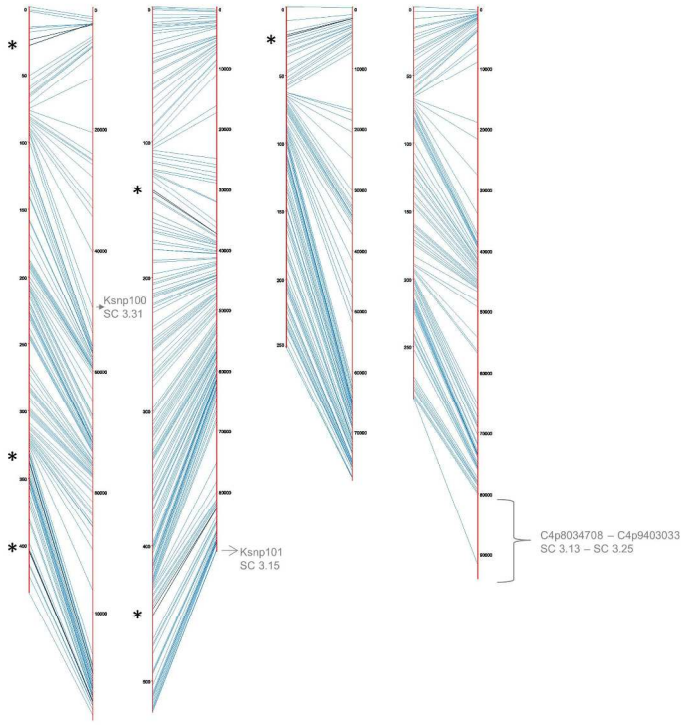

Alignment of the linkage map (left side) to the reference genome RRES v4.0 (right side). The dark stars and the black lines represent the six inversions remaining in the linkage map. The location of the sequence placed by King et al. in the assembly and anchored by the linkage map is indicated in grey.

254x190mm (300 x 300 DPI)

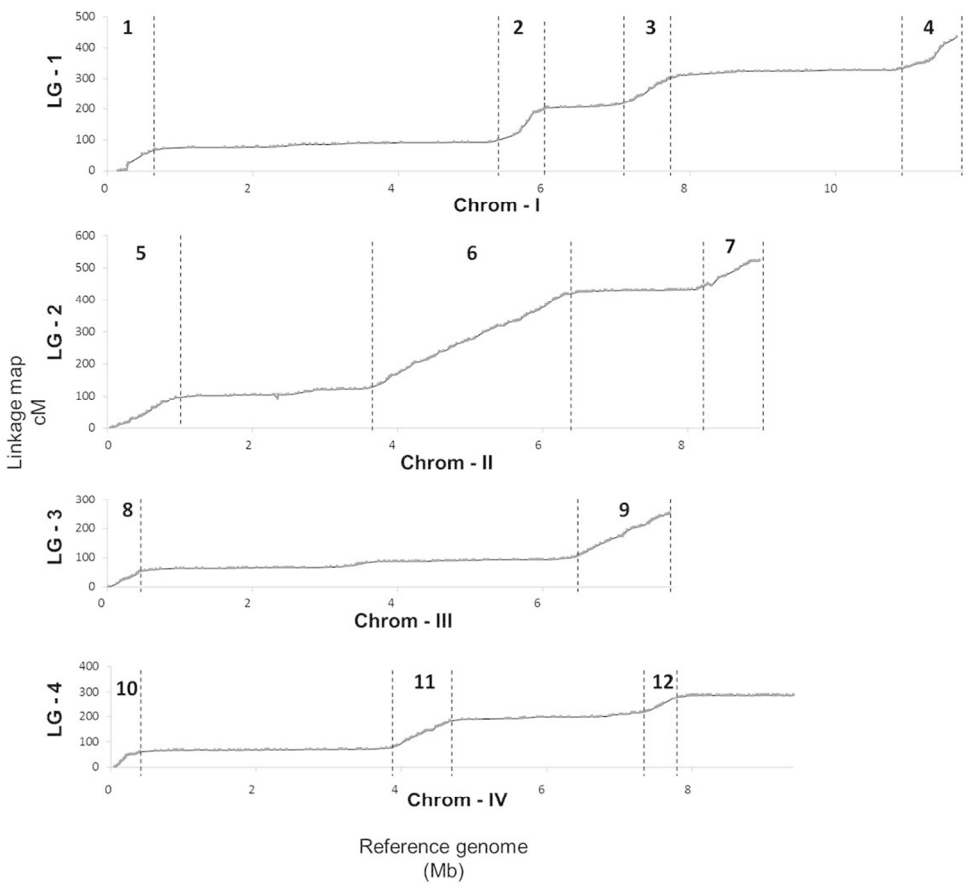

Figure 3: Scatterplot showing the linkage map position (y-axis) and physical position (x-axis). The dotted lines delimitate recombinant-active sections (numbered with arabic numerals) from recombinant-desert sections.

203x180mm (150 x 150 DPI)

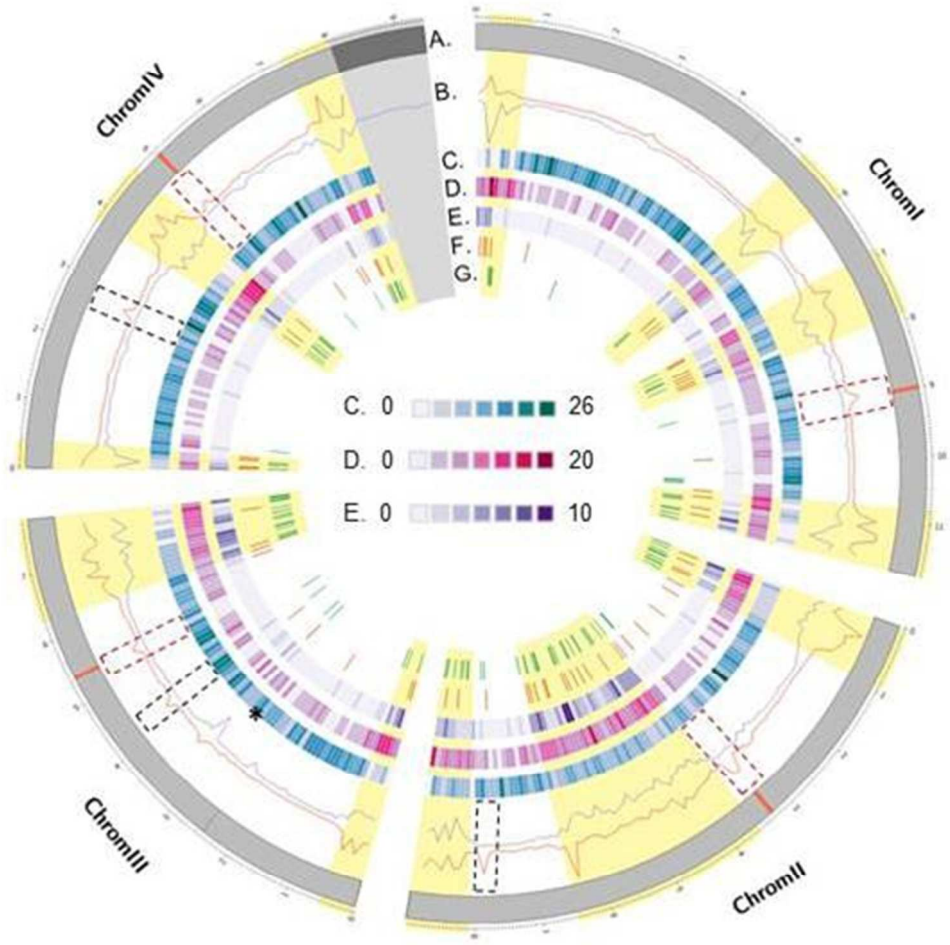

Figure 4: Circos plot of the distribution of several genomic sequence features along the four chromosomes of F. graminearum. A. Representation of the four chromosomes of F. graminearum (in Mb), the dashed red rectangle delimitate the positions of the predicted centromeres. B. In red the SNP density (SNPs/kb) is calculated in windows of 100 kb bins along parental genomes. In blue, the number of CO calculated in separated windows of 100 kb bins across the progeny. The dashed red rectangular boxes locate typical patterns observed at centromere positions; dashed dark boxes locate centromere-like patterns. Recombinant-active sections are highlighted in yellow. C. Protein coding genes expressed constitutively in all planta conditions (Harris et al., 2016). D. Protein coding genes expressed in host-specific conditions (Harris et al., 2016). For C and D, gene density was calculated in 100 kb bin windows E. Location of genes predicted to code for secreted proteins (Brown et al., 2012; King et al., 2015). F. Location of predicted secondary metabolite clusters (Sieber et al., 2014). G. Location of genes showing evidence of diversification.

152x152mm (93 x 93 DPI)

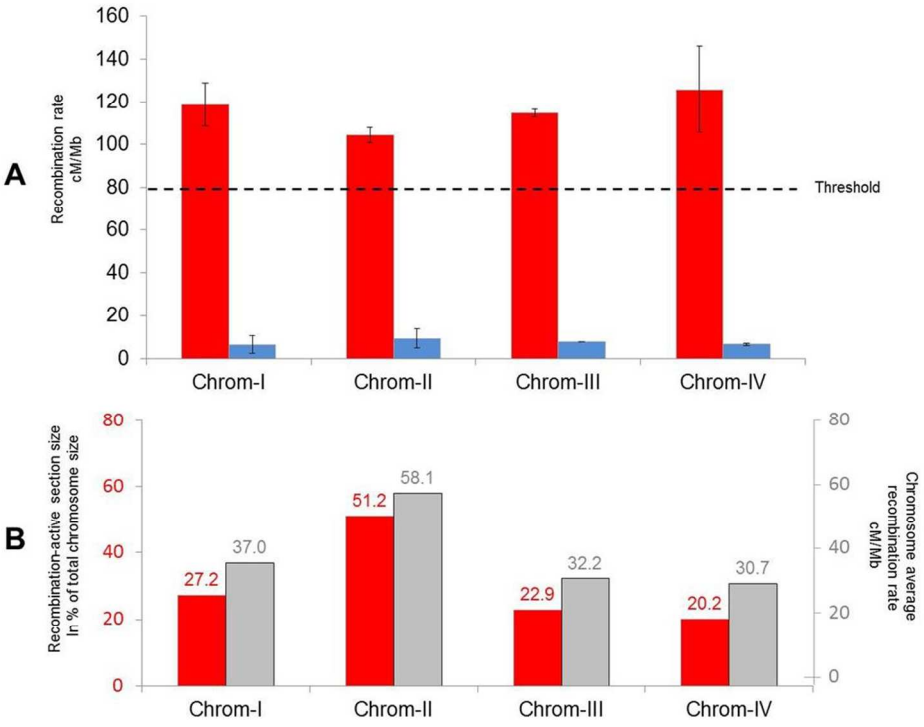

Figure 5: A. Recombination rate distribution according to chromosomal section. Recombinant-active sections are given in red, and recombinant-desert sections in blue. The dashed line refers to the recombination rate threshold to be considered as recombinant-active section (2-fold increase of genome-wide recombination rate). B. The percentage of total size of chromosome allocated to recombinant-active sections is given in red, and the chromosome average recombination rate (cM/Mb) in grey.

203x148mm (150 x 150 DPI)